2023

Rate of Change of Direct-Axis Current Component Protection Scheme for Inverter-Based Islanded Microgrids

Abdolhamid Farshadi

Behzad Keyvani Eydi

Hamed Nafisi

See next page for additional authors

Authors

Abdolhamid Farshadi, Behzad Keyvani Eydi, Hamed Nafisi, Hossein Askarian-Abyaneh, and Arash Beiranvand

IEEE Access
Multidisciplinary | Rapid Review | Open Access Journal

Received 20 April 2023, accepted 26 April 2023, date of publication 2 May 2023, date of current version 17 May 2023.

Digital Object Identifier 10.1109/ACCESS.2023.3272502

RESEARCH ARTICLE

Rate of Change of Direct-Axis Current Component Protection Scheme for Inverter-Based Islanded Microgrids

ABDOLHAMID FARSHADI[1], BEHZAD KEYVANI EYDI[2], HAMED NAFISI[1], HOSSEIN ASKARIAN-ABYANEH[1], (Member, IEEE), AND ARASH BEIRANVAND[3], (Member, IEEE)

[1]Department of Electrical Engineering, Amirkabir University of Technology, Tehran 1591634311, Iran
[2]School of Electrical and Electronics Engineering, University College Dublin (UCD), Dublin 4, D04 V1W8 Ireland
[3]School of Electrical and Electronic Engineering, Technological University Dublin, Dublin 7, D07 EWV4 Ireland

Corresponding authors: Hamed Nafisi (nafisi@aut.ac.ir) and Arash Beiranvand (arash.beiranvand@tudublin.ie)

ABSTRACT Rapid growth in the utilization of the inverter-interfaced distributed energy resources (IIDERs) in microgrids has brought new challenges in the network protection area. Microgrid protection specifically becomes a concern during operation in the islanded mode. There is a considerable reduction in fault current levels in this mode compared to when the microgrid is connected to the grid, which makes conventional algorithms operate with significant delay or, in many cases, not even pick up the fault. This paper proposes a protection algorithm based on the rate of change of direct-axis current component (i_d) to protect inverter-based microgrids (IBMGs). The proposed algorithm is applicable for microgrids with centralized protection as well as those deploying a decentralized approach equipped with the unit protection of the relevant lines. Photovoltaic (PV) systems and battery energy storage systems (BESS) are taken into account in this research and modeled precisely to capture the high-frequency effects of power-electronic converters and investigate the response of IIDERs in fault conditions. The effectiveness of the proposed protection method will be evaluated by applying symmetrical and asymmetrical faults in different locations with different resistances simulated on a test IBMG system in PSCAD/EMTDC environment. In addition, protection robustness against non-fault conditions such as a sudden increase in load levels, environmental uncertainties, and noisy measurement conditions will be scrutinized.

INDEX TERMS Fault detection, inverter-based microgrid, microgrid protection, rate of change of i_d (RoCoId).

NOMENCLATURE

i_d/i_q	Direct/quadrature axis current components [A].
v_d/v_q	Direct/quadrature axis voltage components [V].
i_d^*/i_q^*	Reference direct/quadrature axis current components [A].
v_d^*/v_q^*	Reference direct/quadrature axis voltage components [V].
P^*/P	Reference/measured values of active power [W].
Q^*/Q	Reference/measured values of reactive power [VAr].
V_{dc}^*/V_{dc}	Reference/measured values of dc link voltage [V].
I_{dc}^*/I_{dc}	Reference/measured values of dc link current [A].
V_H	Output voltage of the DC/DC boost converter [V].
I_H	Output current of the DC/DC boost converter [A].
V_{pv}	Output voltage of the PV system [V].
I_{pv}	Output current of the PV system [A].
P_{DC}	DC link power [W].

The associate editor coordinating the review of this manuscript and approving it for publication was Qiang Li.

V_{ref}	Reference voltage generated by MPPT [V].
P_{ref}	Reference power generated by MPPT [W].
L	LCL filter inductor [H].
ω	Microgrid frequency [rad/sec].
θ	Reference angle [rad].
V_{bat}	Battery terminal voltage [V].
E_{bat}	Open circuit voltage of the battery [V].
R_{int}	Internal resistance of the battery [Ω].
I_{bat}	Battery charging current [A].
q	Battery capacity [Ah].
SOC	State of charge [%].
K	Polarization voltage coefficient.
A	Exponential voltage coefficient [V].
B	Exponential capacity coefficient $[(\text{Ah})^{-1}]$.
ω^*	Reference frequency of the microgrid [rad/sec].
v^*	Reference voltage of the microgrid [V].
m/m_d	Frequency droop/damping gain.
n/n_d	Voltage droop/added proportional gain.
T_θ	Dq0 transformation matrix.
Y	Admittance matrix of a network with N buses [Ω].
I	Current matrix of a network with N buses [A].
V	Voltage matrix of a network with N buses [V].
I_d/I_q	Direct/quadrature current matrix of a network with N buses [A].
V_d/V_q	Direct/quadrature voltage matrix of a network with N buses [V].
T	Time period [sec].
a	Multiplication factor.
RoCoId	Rate of change of i_d [A/sec].
$\text{RoCoId}_{max,nf}$	Maximum RoCoId among all relays during non-fault conditions [A/sec].
$\text{RoCoId}_{SLC,i}$	RoCoId of relay i during sudden load change scenarios [A/sec].
$\text{RoCoId}_{IF,i}$	RoCoId of relay i during irradiation fluctuation scenarios [A/sec].
RoCoId_{th}	Threshold value for RoCoId in a microgrid [A/sec].

I. INTRODUCTION

The penetration of the distributed generations (DGs) has been increasing dramatically in recent years due to their economic benefits, environmental concerns and the rise in electricity demand. Indeed, DGs' operation in distribution networks and, specifically microgrids, has had many advantages, such as reducing power losses, increasing reliability, and improving power quality [1], [2], [3]. Despite these advantages, DGs' utilization on a large scale has brought some serious protection issues. These issues become more challenging in inverter-based microgrids(IBMGs) [4], [5]. Unfortunately, there is no efficient and reliable strategy associated with this type of microgrids, and as a consequence, the utilization of this beneficial technology has been limited. The short circuit level in the islanded mode of IBMGs is much lower than the grid-connected mode. This issue results in the mal-operation of conventional overcurrent protection schemes in these systems [6], [7].

Numerous methods have been proposed to resolve problems associated with operating IBMGs in islanded mode. In [8], the dq0 transformation is utilized for converting the phase voltages to dq values and based on these values, the fault is then detected by the under-voltage logic. Meanwhile, this approach may be problematic from discrimination as well as coordination aspects, as the voltage is usually dropped widely and uniformly in the network during the fault. In [9], a protection method based on negative sequence component considering short circuit behavior of grid-forming IIDERs is presented. However, utilization of negative sequence component in conditions such as occurrence of three-phase faults and presence of unbalanced and nonlinear loads may face challenges. Also, using voltage to detect fault location is challenging due to the slight voltage difference between adjacent buses in IBMGs. These issues can be resolved using impedance [10] and admittance-based algorithms [11]. However, these methods are generally not entirely effective in distribution networks with short lines with low levels of X/R ratio. In research [12], the faulted section is determined by comparing the phase difference between the pre-fault and fault current components. This scheme requires prior knowledge of pre-fault power flow direction and also needs a separate method to detect the occurrence of a fault. In [13], the comparison of the phase difference between the positive-sequence current fault component and pre-fault bus voltage is used to detect and isolate the faulty line in IBMGs. However, noise immunity and the performance of the scheme during non-fault conditions such as sudden load changes has not been investigated. Optimization techniques such as genetic algorithm and particle swarm optimization were proposed in [14] and [15] to improve the tripping characteristics of overcurrent relays. However, usage of overcurrent relays may not be effective due to changeable topologies of IBMGs and limited fault current of IIDERs. Adaptive protection is another proposed method for protecting microgrids [16], [17], [18], [19]. In [16], clustering is used to reduce different states of a network and determine settings for each cluster. Different setting groups can also be utilized according to the network modes and conditions [17], [18], [19]. However, all of these methods require centralized protection and extensive communications links. The protection algorithm can be based on harmonics, too. In [20], a percentage of the fifth harmonic component can be injected to fault location in IBMGs by the inverter-interfaced distributed energy resources (IIDER) control system, and then microprocessor-based relays can detect and isolate the fault. Using the concept of differential protection and extracting several features of the fault current

is another method for protecting IBMGs [21], [22], [23], [24], [25], [26]. Data mining and wavelet transform are utilized in [21] and [22] for fault detection, respectively. In [23], the fault is detected by measuring the off-nominal frequency injected by IIDERs. In [24], by generating harmonic voltages through IIDER controllers and creating a new current flow layer, a harmonic-based overcurrent protection scheme for islanded IBMGs is proposed. In these methods, noise immunity and high capital costs for the equipment are the primary concerns. In [25], a method for fault detection has been proposed based on fault current modulation, extraction of the fundamental component and inter harmonic components, and analysis of inter harmonic components. In [26], the differential energy derived from both three-phase current and its zero sequence current component through a machine learning based model, the extreme gradient boost, is used to detect and classify faults in microgrids. Meanwhile, these methods depends on communication links and advanced relays.

According to the aforementioned studies, the main gaps in the previous protection methods can be expressed as the inconsistency in detection and discrimination of the faulty part due to the wide range of disturbances, ignoring the behavior of different types of IIDERs in fault and non-fault cases, and unheeding bi-directional fault currents in IBMGs. In order to resolve the above-mentioned gap, first, dynamic models are utilized for the photovoltaic (PV) systems and battery energy storage systems (BESS) with their associated power electronic control systems. Then, a protection method based on the rate of change of direct-axis current component (RoCoId) for IBMGs is proposed. The key contributions of the proposed method are as follows.

- Utilization of RoCoId for fast and accurate fault detection and discrimination in islanded IBMGs due to the significant difference in its behavior during fault and non-fault conditions.
- Considering the short circuit behavior of both voltage-frequency controlled inverter-interfaced resources (VF-IIDER) and active-reactive power controlled inverter-interfaced resources (PQ-IIDER).
- Maintaining robustness against common operational transients such as sudden load changes, irradiation fluctuations, and noisy measurement conditions.
- Implementation of the proposed method in a centralized and decentralized approach in islanded IBMGs.

The effectiveness of the proposed protection method is verified using the PSCAD/EMTDC software. In addition, a comparison between previous protection techniques and the proposed method is presented in Table.1. It is worth noting that in terms of practicality, the implementation of the proposed method, like most of the effective methods mentioned in Table.1, is somewhat costly. However, the benefits it provides outweigh this disadvantage.

This paper consists of six sections: PV system and BESS modelling are presented in section II. The main concepts of the proposed protection method are introduced in section III. The simulation results and the effectiveness of the proposed approach are shown in section IV. The possibility of mal-operation and the method's robustness is scrutinized in section V, and finally, the conclusions and further recommendations of the work are given in section VI.

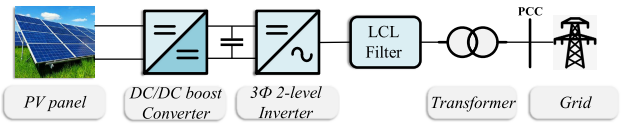

FIGURE 1. General structure of PV system integration to a grid.

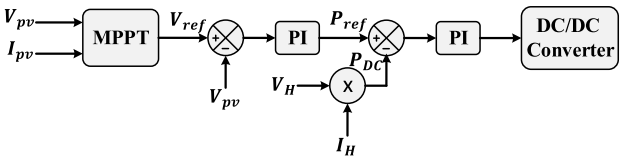

FIGURE 2. DC/DC Converter control block diagram of PV system.

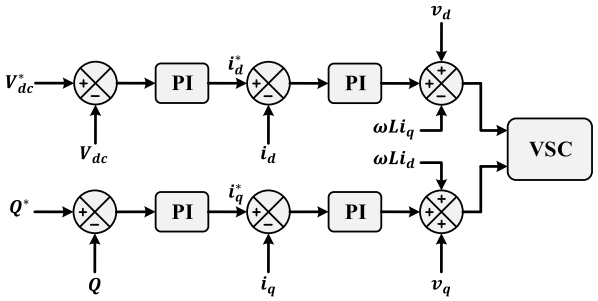

FIGURE 3. Inverter control block diagram of PV system.

II. PV SYSTEM AND BESS MODELLING

In this part, the details of dynamic models for PV systems and BESS utilized for this study have been represented. These models will be later utilized in the test case in order to evaluate the proposed protection scheme.

A. PV SYSTEM

The general schematic for a PV system integrated with a grid is shown in Fig.1. The PV system is connected to the grid through a DC/DC boost converter, a three-phase 2-level inverter, an LCL filter, and a transformer.

The DC/DC boost converter control block diagram used in Fig.1 is shown in Fig.2. Maximum available solar power can be achieved by maximum power point tracking (MPPT) functionality. Here, MPPT is based on an incremental conductance algorithm. As can be seen from Fig.2, the output voltage and current of the PV system are passed to the MPPT block, which generates the reference voltage (V_{ref}). Thereupon, V_{ref} is compared to V_{pv} and the error signal is given to a PI controller to generate reference power (P_{ref}). V_H and I_H are symbols for output voltage and current of the DC/DC boost converter and as shown in this figure, P_{ref} is compared to the dc link power (P_{DC}), and the error signal is given to a PI controller to generate the boost converter duty cycle.

The inverter control block diagram is depicted in Fig.3. In this voltage source converter (VSC), the reference values of

TABLE 1. Comparison of proposed method with previous protection techniques.

Methodology	Modeled DER types	Fault detection & discrimination (Accuracy)	Noise immunity	Non-fault conditions	Fault detection speed	Implementation cost	Communication infrastructure
Differential frequency protection [23]	PQ-IIDER VF-IIDER	Effective	Not proven	Unexamined	One cycle	Expensive	Needed
Interharmonic differential protection [25]	PQ-IIDER VF-IIDER	Effective	Not proven	Unexamined	Two cycles	Expensive	Needed
Differential energy based protection [18]	SBDER* PQ-IIDER	Effective	Immune	Examined	Two cycles	Expensive	Needed
Voltage-based protection [8]	PQ-IIDER	Not effective	Immune	Unexamined	One cycle	Expensive	Needed
Voltage restrained negative sequence protection [9]	VF-IIDER	Not effective	Immune	Examined	Whithin a cycle	Expensive	Needed
Optimized overcurrent protection [16]	PQ-IIDER	Not effective	Immune	Unexamined	One cycle	Reasonable	Not needed
Impedance-based protection [10]	PQ-IIDER	Not effective	Immune	Unexamined	One cycle	Expensive	Needed
Phase comparison of voltage & current [13]	PQ-IIDER	Effective	Immune	Unexamined	Two cycles	Expensive	Needed
Phase comparison of currents [12]	PQ-IIDER	Effective	Not proven	Unexamined	Two cycles	Reasonable	Needed
Superimposed adaptive of voltage & current [19]	SBDER PQ-IIDER	Not effective	Immune	Unexamined	One cycle	Reasonable	Not needed
Harmonic injection based protection [24]	PQ-IIDER	Effective	Not proven	Examined	One cycle	Expensive	Not needed
Proposed method	VF-IIDER PQ-IIDER	Effective	Immune	Examined	Whithin a cycle	Expensive	Needed

* Synchronous-based distributed energy resources

i_d and i_q are generated through two independent control loops by regulating the dc link voltage (V_{dc}) and reactive power (Q). In this figure, L and ω represent the LCL filter inductor and microgrid frequency, and the terms $\omega L i_d$ and $\omega L i_q$ are used for eliminating cross terms and enabling straightforward tuning of the loop parameters. The inverter switching control is performed by comparing the reference values of i_d and i_q with values calculated later via (3) and (4).

B. BESS

In this paper, the lead-acid battery model is utilized. Nonlinear elements of the battery are also included in the model. The variation in battery terminal voltage during charge and discharge processes is a function of the state of charge (SOC) and temperature of the electrolyte. Battery terminal voltage (V_{bat}) and SOC can be written as follows [27].

$$V_{bat} = E_{bat} + R_{int} I_{bat} - K\frac{q}{q + \int I_{bat} dt} + Ae^{B\int I_{bat} dt} \quad (1)$$

$$SOC = 100\left(1 + \frac{\int I_{bat} dt}{q}\right) \quad (2)$$

where E_{bat} is the open-circuit voltage of the battery, R_{int} is the internal resistance of the battery, and I_{bat} is the current flowing through the battery. The polarization effect is also considered in the third term of (1), with K as the polarization coefficient, and q as the battery capacity. In the fourth term, A and B are the coefficients of the exponential function of voltage and capacity. These parameters can be extracted from a manufacturer's discharge curve [28].

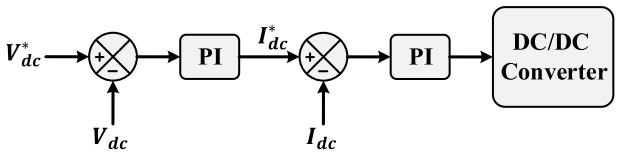

FIGURE 4. DC/DC converter control block diagram of BESS in islanded mode.

In this research, BESS is connected to the grid through a bidirectional DC/DC converter and a three phase 2-level inverter (Fig.4). In islanded mode, DC link voltage is adjusted by the DC/DC converter and the microgrid frequency and voltage are controlled by the inverter. The latter is performed by a method called proportional-derivative droop control with which power sharing is also handled. It is similar to conventional droop control method, with an exception on insertion of a damping controller in frequency control path in order to weaken existing power oscillation. The inverter control block diagram is shown in Fig.5 [29].

III. PROPOSED PROTECTION METHOD

IIDGs dynamics are relatively fast, and evaluation based on the quasi-static or time-varying phasors, i.e. RMS

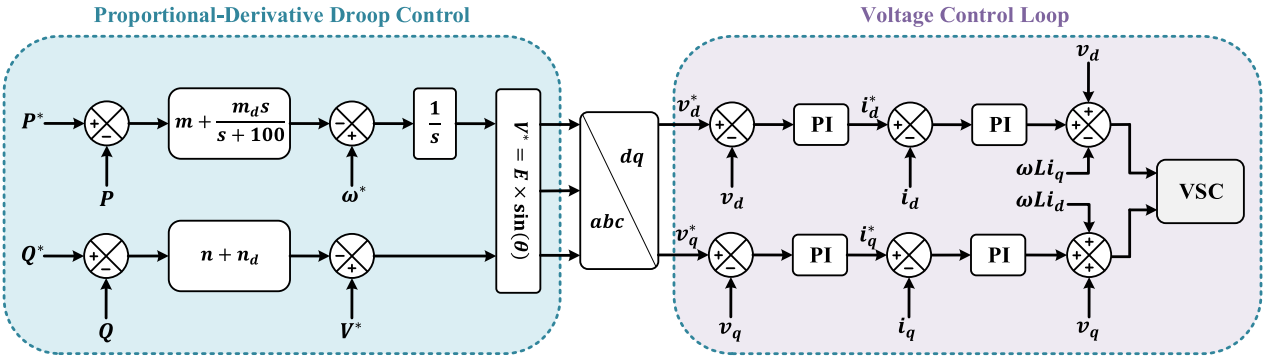

FIGURE 5. Inverter control block diagram of BESS in islanded mode.

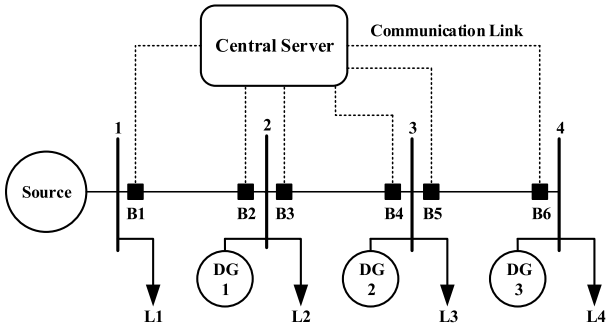

FIGURE 6. Sample microgrid equipped with communication system and central server.

simulations, cannot be applicable for this study, and instead, techniques that take into account the electromagnetic transients should be utilized. Moreover, dq0 model, direct axis current component (i_d) as well as rate of change of i_d (RoCoId) are used in the proposed protection method in order to detect fault high-frequency effects observed in IBMGs with low inertia.

A. DQ0 TRANSFORMATION

1) BASIC DEFINITIONS

The main advantage of dq0 transformation is the conversion of AC sinusoidal components to constant values. Resistors, inductors, capacitors and other elements of the power system can also be modelled with this transformation.

The dq0 transformation and the relevant inverse matrix are defined in (3) to (5). In these equations, θ is the reference angle [30].

$$x_{abc}=\begin{bmatrix} x_a \\ x_b \\ x_c \end{bmatrix}, x_{dq0}=\begin{bmatrix} x_d \\ x_q \\ x_0 \end{bmatrix};$$
$$x_{dq0} = T_\theta x_{abc}, x_{abc} = T_\theta^{-1} x_{dq0} \tag{3}$$
$$T_\theta = \frac{2}{3}\begin{bmatrix} \cos(\theta) & \cos\left(\theta-\frac{2\pi}{3}\right) & \cos\left(\theta+\frac{2\pi}{3}\right) \\ -\sin(\theta) & -\sin\left(\theta-\frac{2\pi}{3}\right) & -\sin\left(\theta+\frac{2\pi}{3}\right) \\ \frac{1}{2} & \frac{1}{2} & \frac{1}{2} \end{bmatrix} \tag{4}$$

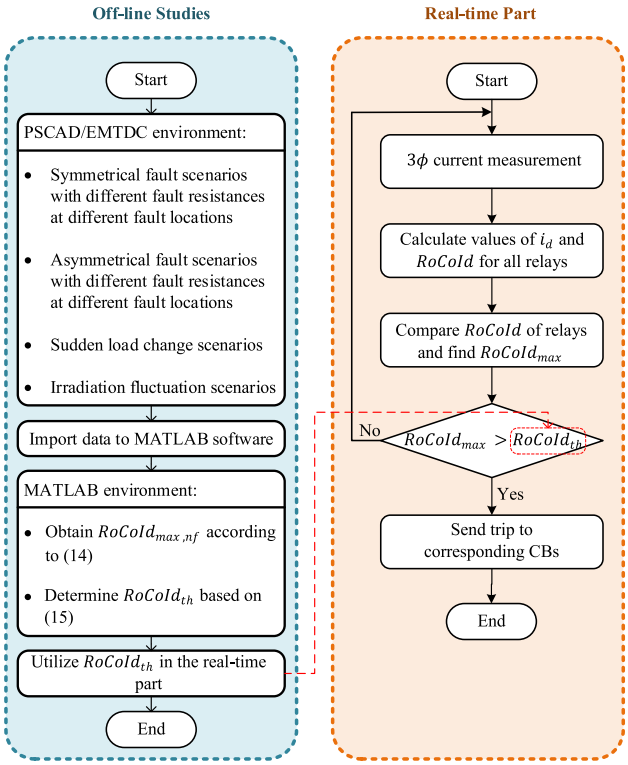

FIGURE 7. Flowchart of centralized implementation.

$$T_\theta^{-1} = \begin{bmatrix} \cos(\theta) & -\sin(\theta) & 1 \\ \cos\left(\theta-\frac{2\pi}{3}\right) & -\sin\left(\theta-\frac{2\pi}{3}\right) & 1 \\ \cos\left(\theta+\frac{2\pi}{3}\right) & -\sin\left(\theta+\frac{2\pi}{3}\right) & 1 \end{bmatrix} \tag{5}$$

2) ADVANTAGES OF USING DQ0 PARAMETERS IN IBMGs

dq0 transformation is an extension to the time-varying phasor model [30]. To compare these two models, consider a symmetrical network consisting of N buses. This grid is described by admittance matrix Y(s). In a quasi-static system, network equations are as follows:

$$I = Y(j\omega_s)V \tag{6}$$

For quasi-static systems, (6) can be rewritten as the following equation, considering the admittance matrix as constant

and evaluated at a single frequency $s = j\omega_s$:

$$\begin{bmatrix}\mathrm{Re}\{I\}\\ \mathrm{Im}\{I\}\end{bmatrix}=\begin{bmatrix}\mathrm{Re}\{Y(j\omega_s)\}-\mathrm{Im}\{Y(j\omega_s)\}\\ \mathrm{Im}\{Y(j\omega_s)\}\ \ \mathrm{Re}\{Y(j\omega_s)\}\end{bmatrix}\begin{bmatrix}\mathrm{Re}\{V\}\\ \mathrm{Im}\{V\}\end{bmatrix} \tag{7}$$

To generalize these results to networks that are not quasi-static, such as inverter-based microgrids, using $\theta = \omega_s t$, the network equations can be expanded as (8), where the values of $N_1(s)$ and $N_2(s)$ are given in (9) and (10) [30]:

$$\begin{bmatrix}I_d(s)\\ I_q(s)\end{bmatrix}=\begin{bmatrix}N_1(s) & jN_2(s)\\ -jN_2(s) & N_1(s)\end{bmatrix}\begin{bmatrix}V_d(s)\\ V_q(s)\end{bmatrix} \tag{8}$$

$$N_1(s)=\frac{1}{2}\left(Y(s+j\omega_s)+Y(s-j\omega_s)\right) \tag{9}$$

$$N_2(s)=\frac{1}{2}\left(Y(s+j\omega_s)-Y(s-j\omega_s)\right) \tag{10}$$

At lower frequencies ($s\to 0$), (9) and (10) can be simplified to (11) and (12).

$$N_1(s)\approx\frac{1}{2}\left(Y(j\omega_s)+Y^*(j\omega_s)\right)=\mathrm{Re}\{Y(j\omega_s)\} \tag{11}$$

$$N_2(s)\approx\frac{1}{2}\left(Y(j\omega_s)-Y^*(j\omega_s)\right)=\mathrm{jIm}\{Y(j\omega_s)\} \tag{12}$$

In this case, the dq0 model and the model used in quasi-static networks are equal. Therefore, the dq0 model is a generalization of the quasi-static model and is applicable to a wider range of frequencies. Meanwhile, networks that are not quasi-static, such as IBMGs, have a wider frequency range in the transient state and cannot be accurately described by the time-varying phasor model [31]. It is the main motivation for consideration of the high-frequency effects through evaluation of i_d and relevant rate of change (RoCoId) in the proposed scheme.

B. PROPOSED PROTECTION SCHEME

1) CENTRALIZED APPROACH

Many protection schemes, especially in microgrid protection, are based on extensive communication links. Fig.6 shows a sample microgrid equipped with a communication system in which the information of all relays is sent to the central server and, then after fault occurrence, the central server detects the location of the fault by comparing the information sent from all relays. In this paper, fault location is detected by comparing RoCoId sent by all relays and finding the relay that has the maximum RoCoId. RoCoId is calculated within a half cycle for each relay through (13) by the central server. To determine the threshold value for RoCoId, first, in offline studies, various simulations are performed on the studied microgrid in the PSCAD/EMTDC software environment during sudden load changes, irradiation fluctuations, and the occurrence of various faults in different locations with different resistances. Then, by transferring the data of these simulations to MATLAB software, RoCoId is calculated for all relays in all different simulated scenarios. According to the calculated values, the maximum value of RoCoId is extracted from all non-fault conditions based on (14), where $\mathrm{RoCoId}_{SLC,i}$ is the RoCoId of relay i during sudden load change scenarios, $\mathrm{RoCoId}_{IF,i}$ is the RoCoId of relay i during irradiation fluctuation scenarios, and $\mathrm{RoCoId}_{max,nf}$ is the maximum RoCoId among all relays during non-fault conditions. Due to the significant difference between the value of RoCoId in fault and non-fault conditions, (15) is used to determine the threshold value for RoCoId in the studied microgrid. For secure and selective protection, and by considering a safety margin, the multiplication factor (a) is identified as 6. The specified threshold is linked to the real-time part and in case of changes in the structure and nominal values of the microgrid, its value will also change.

$$\mathrm{RoCoId}=\frac{di_d}{dt}=\frac{i_d(t+T/2)-i_d(t)}{T/2} \tag{13}$$

$$\mathrm{RoCoId}_{max,nf}=max\{\mathrm{RoCoId}_{SLC,i},\mathrm{RoCoId}_{IF,i}\} \tag{14}$$

$$\mathrm{RoCoId}_{th}=a.\mathrm{RoCoId}_{max,nf} \tag{15}$$

If the maximum value of RoCoId is greater than the fixed threshold value, the central server sends the command to open the breaker of the associated relay as well as the adjacent breaker on the same line. Therefore, the faulty line will be removed from the network. It should be noted that during high impedance faults (higher than 300Ω), the fault current injected by IIDER would be extremely small and thus, the RoCoId value will not come into action. The flowchart for centralized implementation is depicted in Fig.7.

2) DECENTRALIZED IMPLEMENTATION

In a decentralized implementation, trip decisions are made by protective relays associated with the lines equipped with communication links between two ends. In this approach, RoCoId can be incorporated in a hybrid algorithm with a directional function (Fig.8). In this case, when a fault is detected in the forward direction by the directional element, and simultane-

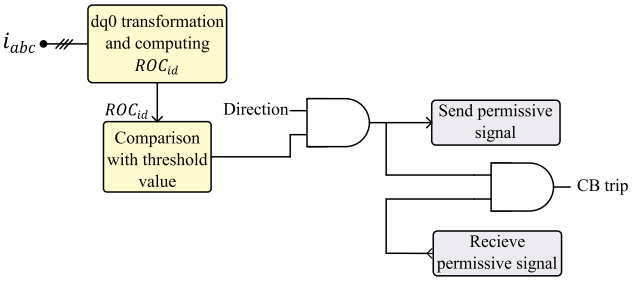

FIGURE 8. Logic diagram of proposed relay for the decentralized approach.

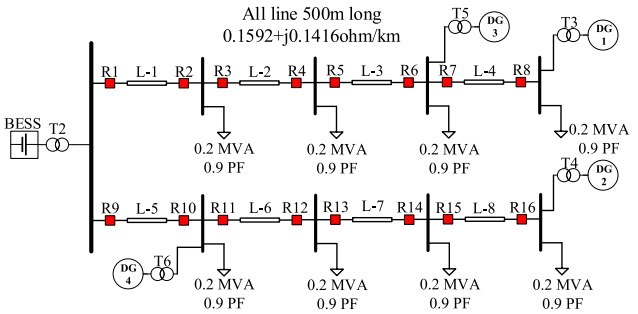

FIGURE 9. Test system.

TABLE 2. RoCoId during various fault occurrences.

Fault type & location	Relay	RoCoId(A/s) within a half cycle $R_f=0.01\Omega$	$R_f=10\Omega$	Fault type & location	Relay	RoCoId(A/s) within a half cycle $R_f=0.01\Omega$	$R_f=10\Omega$	Fault type & location	Relay	RoCoId(A/s) within a half cycle $R_f=0.01\Omega$	$R_f=10\Omega$
	R1	6131.5	4913.2		R1	4647.3	3394.9		R1	4673.2	3918.3
	R2	6152.1	4912.7		R2	4450.9	3327.1		R2	4674.0	3918.9
	R3	7363.4	5988.2		R3	3369.8	2114.0		R3	3729.2	2928.2
	R4	7362.7	5988.1		R4	3370.1	2118.6		R4	3729.6	2927.9
	R5	8595.0	7093.3		R5	2290.5	1435.3		R5	2786.9	1935.0
	R6	3643.4	2852.0		R6	2290.6	1435.9		R6	2786.4	1934.1
	R7	1824.4	1423.7		R7	1144.5	859.1		R7	1389.9	1068.8
ABC-G	R8	1824.5	1424.2	A-G	R8	1144.7	858.7	AB	R8	1390.0	1070.3
(50% of	R9	6044.8	4888.1	(30% of	R9	4455.0	3105.6	(90% of	R9	4524.3	3950.4
line3)	R10	6041.5	4889.2	line1)	R10	4455.6	3106.7	line8)	R10	4524.6	3950.8
	R11	4247.4	3533.1		R11	3303.2	2668.0		R11	5954.3	4924.3
	R12	4248.3	3533.2		R12	3303.6	2668.5		R12	5953.7	4923.6
	R13	3018.9	2440.6		R13	2223.0	1607.2		R13	6903.2	5920.0
	R14	3019.3	2440.1		R14	2222.5	1607.6		R14	6904.3	5919.5
	R15	1814.0	1392.2		R15	1143.9	856.5		R15	7854.1	6927.3
	R16	1815.8	1392.1		R16	1143.8	857.6		R16	1471.5	1101.8

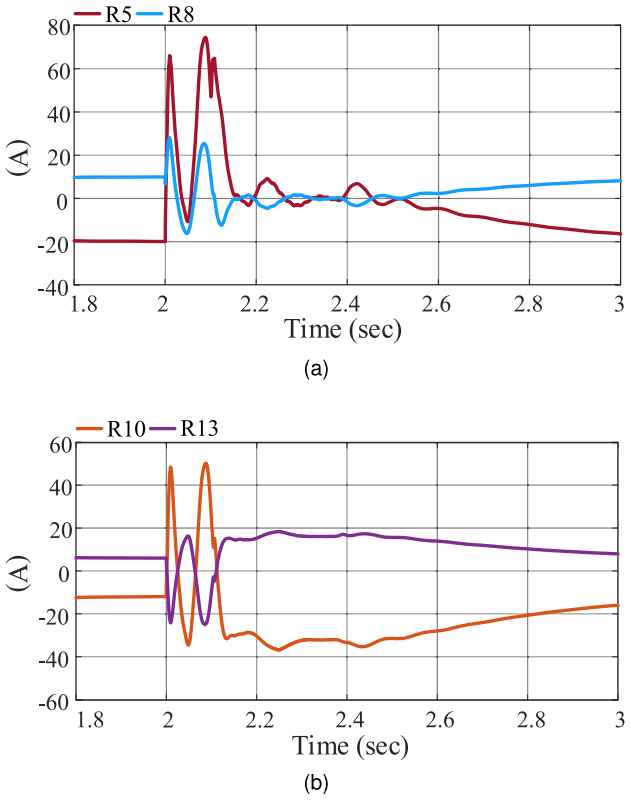

FIGURE 10. (a) i_d values measured with R5 and R8 for ABC-G fault with Rf = 0.01Ω in the middle of line 3, (b) i_d values measured with R10 and R13 for the same fault.

ously RoCoId becomes greater than a preset threshold value, a permissive signal is sent to the adjacent relay located at the other end. At the remote end, the received permissive signal,

TABLE 3. Maximum values of rate of change of id among all relays for various faults.

Fault type	Fault location	Maximum RoCoId(A/s)	Corresponding relay
ABC-G	Line1	6144.6	R1
	Line3	8595.0	R5
	Line6	7934.7	R11
	Line8	10365.0	R15
A-G	Line1	4739.9	R1
	Line3	6365.1	R5
	Line6	5358.3	R11
	Line8	7441.8	R15
AB	Line1	5160.4	R1
	Line3	6528.8	R5
	Line6	6077.0	R11
	Line8	7881.1	R15

together with the local relay decision signal, can set the output of the second AND gate, and in that case, the trip command will be sent to the corresponding breaker, and the faulty line will be disconnected from both ends.

IV. SIMULATION RESULTS

In this section, the performance of the proposed protection method is investigated. In this paper, PSCAD/EMTDC v4.5.0 software and MATLAB version 9.5 (R2018b) software installed on a PC with Intel(R) Core(TM) i5-4200U CPU processor and 4.00 GB installed RAM are used for simulations and calculations. An urban microgrid network in Canada that

TABLE 4. Id and RoCoId values for sudden load change scenario.

Relay	$i_d(A)$		RoCoId(A/s)
	Before load change	After load change	Within a half cycle
R1	12.04	23.76	64.8
R2	-12.017	-23.75	66.8
R3	-3.95	4.81	43.0
R4	3.94	-4.83	44.3
R5	-19.91	-14.04	154.8
R6	19.89	14.11	156.5
R7	-9.95	-7.05	76.8
R8	9.95	7.06	76.8
R9	12.03	23.69	58.3
R10	-12.01	-23.72	61.2
R11	21.98	30.79	138.6
R12	-21.99	-30.77	136.9
R13	5.99	11.84	30.2
R14	-6.00	-11.85	30.7
R15	-9.98	-7.05	77.6
R16	9.96	7.04	79.9

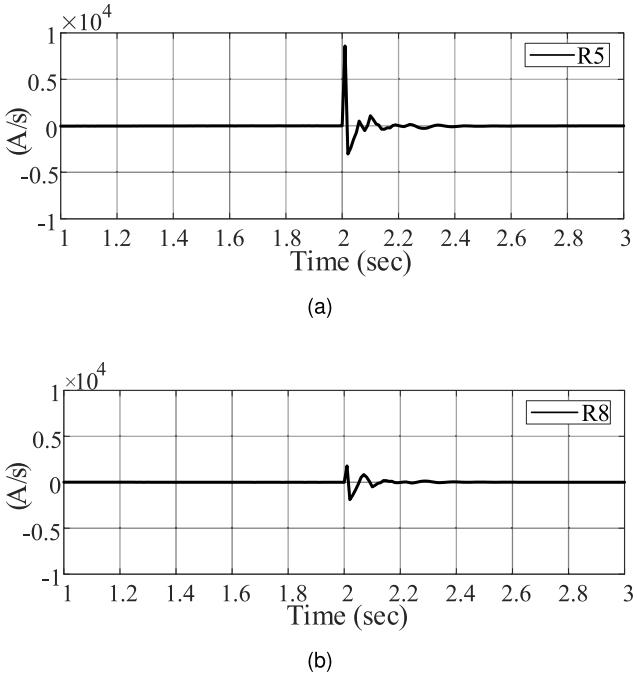

FIGURE 11. (a) RoCoId variation for R5 during ABC-G fault with Rf = 0.01Ω in the middle of line 3, (b) RoCoId variation for R8 during the same fault.

consists of two 12.47kV feeders with a rating of 8 MVA is selected as the test case [32]. It has been implemented with PSCAD/EMTDC software, as shown in Fig.9. In this section, occurrence of various faults in different locations will be studied, and the protection speed, as well as the discrimination in the fault detection, will be investigated.

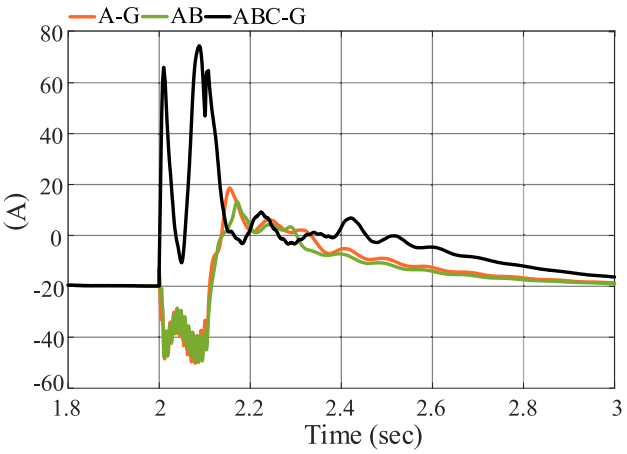

FIGURE 12. The comparison of the i_d diagram during occurrence of an ABC-G fault in the middle of L-3, an A-G fault in the middle of L-1, and an AB fault in the middle of L-8 for R5.

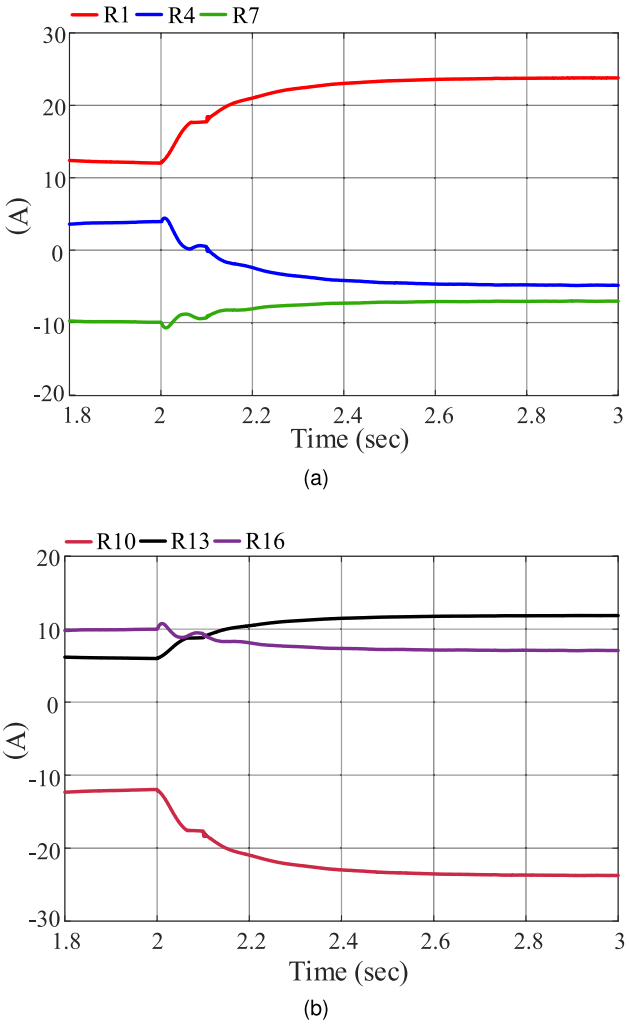

FIGURE 13. i_d for sudden load change scenario (a) measured with R1, R4, and R7 (b) measured with R10, R13, and R16.

The worst-case scenario is studied here, assuming all of the DGs, as well as BESS, are in service through power electronics converters. To determine the threshold value for RoCoId,

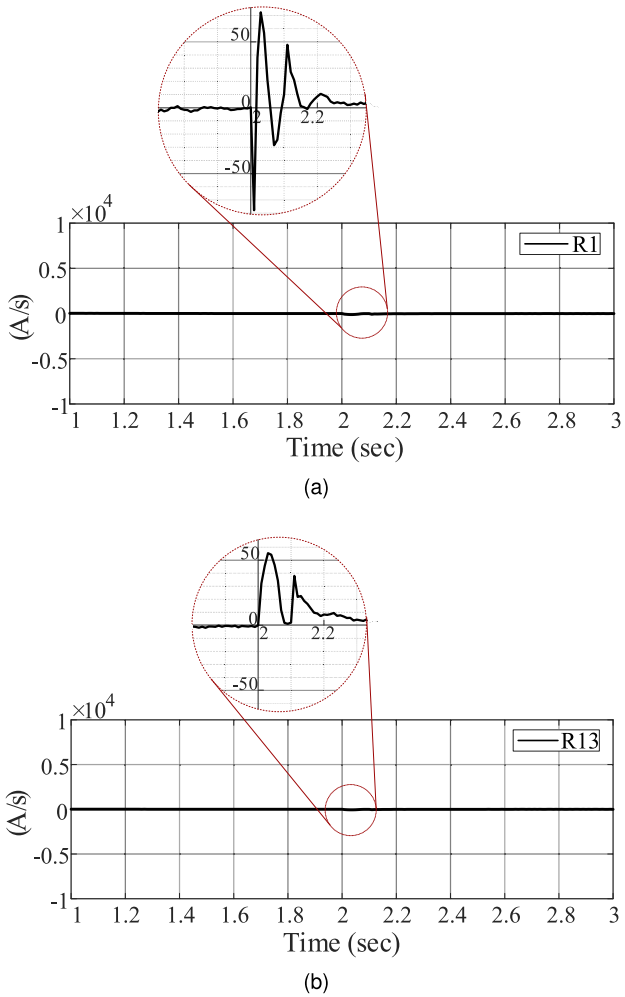

FIGURE 14. (a) RoCoId variation for R1 during sudden load change scenario (b) RoCoId variation for R13 during the same scenario.

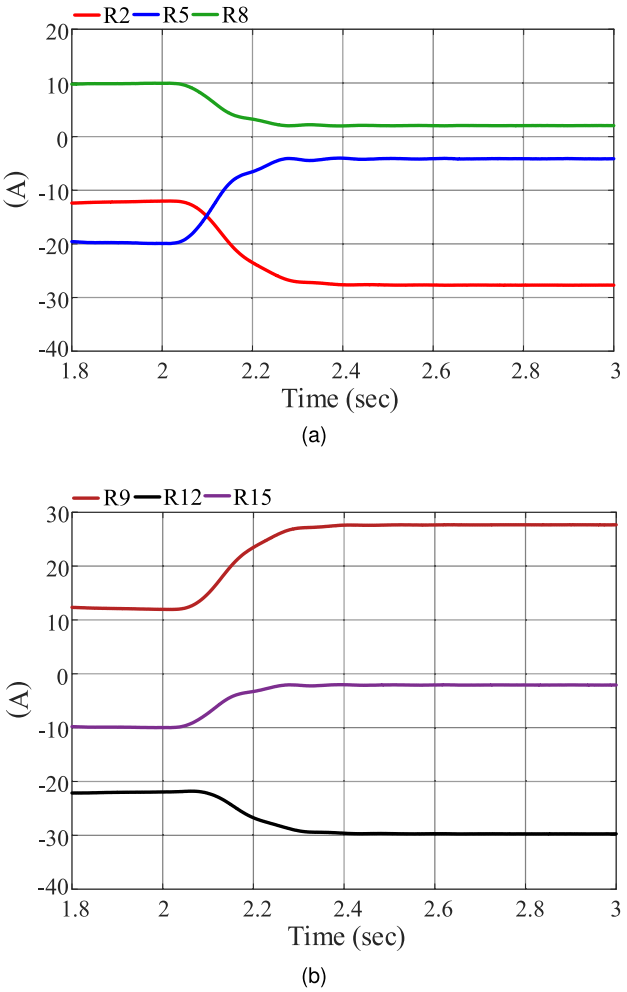

FIGURE 15. i_d for irradiation fluctuation scenario (a) measured with R2, R5, and R8, (b) measured with R9, R12, and R15.

according to the flowchart in Fig.7, in offline-studies, several simulations were performed in non-fault conditions on the test system shown in Fig.9, and some of the results obtained from them are presented in section V. Based on these results, the value of $\text{RoCoId}_{max,nf}$ is determined to be 156.5 A/s, and according to (15), the value of RoCoId_{th} is considered to be 940 A/s for this microgrid. In addition, the microgrid is assumed to operate in steady-state conditions, and the PV systems are in the standard conditions, i.e. irradiation and temperature are 1000 W/m2 and 25 °C, respectively.

In several scenarios, the occurrence of symmetrical and asymmetrical faults with different fault resistances and in different locations on the studied microgrid was evaluated. For instance, the RoCoId values measured by all relays in the microgrid for the occurrence of a three-phase to ground fault with 0.01Ω and 10Ω resistances at 50% of the L-3, the occurrence of a single-phase to ground fault with 0.01Ω and 10Ω resistances at 30% of the L-1, and the occurrence of a phase to phase fault with 0.01Ω and 10Ω resistances at 90% of the L-8 are given in Table.2. The i_d curves measured with R5 and R8 as well as R10 and R13 during the occurrence of a three-phase fault with Rf = 0.01Ω in the middle of L-3 is also shown in Fig.10. In addition, Fig.11 shows the variation of RoCoId for R5 and R8 during the occurrence of the aforementioned fault. Furthermore, the comparison of the i_d diagram during ABC-G fault in the middle of L-3, A-G fault in the middle of L-1, and AB fault in the middle of L-8 is shown in Fig.12. The maximum values of RoCoId measured by all relays during the occurrence of different solid faults in the middle of L-1, L-3, L-6, and L-8 are also brought in Table.3. Based on these simulation results, if the microgrid is equipped with a communication system and a central server, fault will be detected and discriminated within a cycle by the proposed algorithm shown in the flowchart depicted in Fig.7. If the microgrid is not equipped with the centralized protection, with the decentralized approach (Fig.8), it is still possible to take advantage of RoCoId, as can be seen from RoCoId levels brought in Table.2. It is observed that, for instance, AB fault in the middle of L-8 can be detected by R9, R11, R13, R15, and R16 in forward direction, and as a result, the output of the first AND gate sets for these relays. However, only R15 and

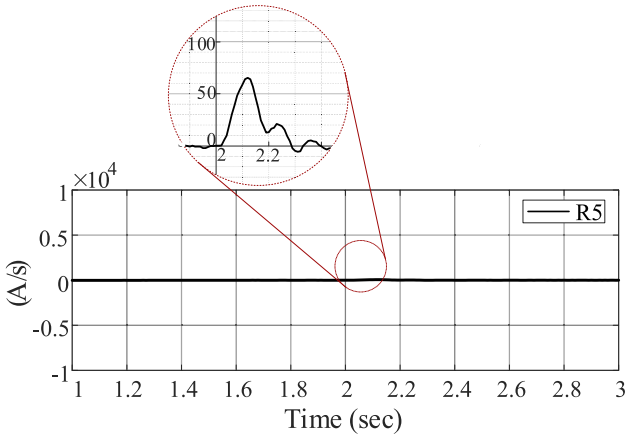

(a)

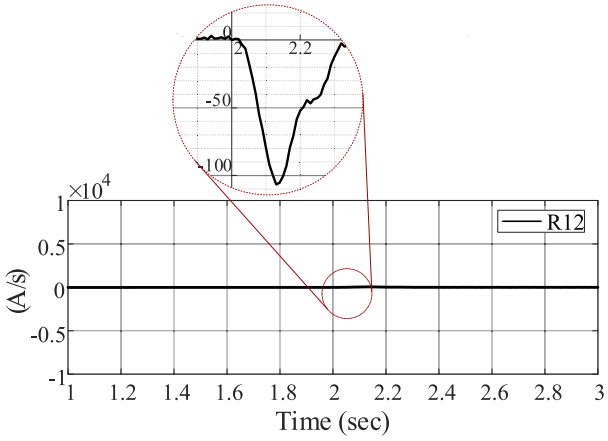

(b)

FIGURE 16. (a) RoCoId variation for R5 during irradiation fluctuation scenario (b) RoCoId variation for R12 during the same scenario.

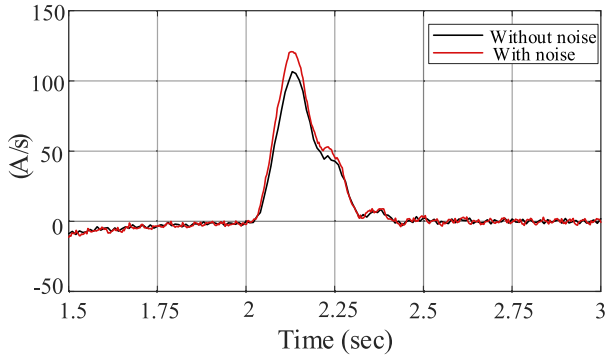

FIGURE 17. RoCoId variation for R11 during irradiation fluctuation scenario with and without noise.

R16 receive the permissive signal from the adjacent relay and send the trip command to the corresponding breakers, and the faulty line will be disconnected from both ends.

V. ROBUSTNESS TEST OF PROPOSED SCHEME

Under regular operational transients, the protection scheme should not cause unreasonable interruption. In the network under study, the most discernable operational transients potentially susceptible to misleading the protection are environmental uncertainties, e.g. irradiation fluctuations and sudden load changes. In this section robustness of the proposed method against these transients will be investigated.

TABLE 5. RoCoId values for irradiation fluctuation scenario.

Relay	RoCoId(A/s) within a half cycle	
	Clean signal	Noisy signal
R1	54.8	64.5
R2	56.9	66.7
R3	41.3	46.8
R4	42.7	48.1
R5	71.5	79.6
R6	72.3	80.3
R7	87.2	91.8
R8	87.4	91.9
R9	51.1	57.2
R10	54.3	60.2
R11	103.7	118.4
R12	103.1	117.2
R13	32.6	36.0
R14	34.0	37.6
R15	92.8	104.2
R16	89.7	102.6

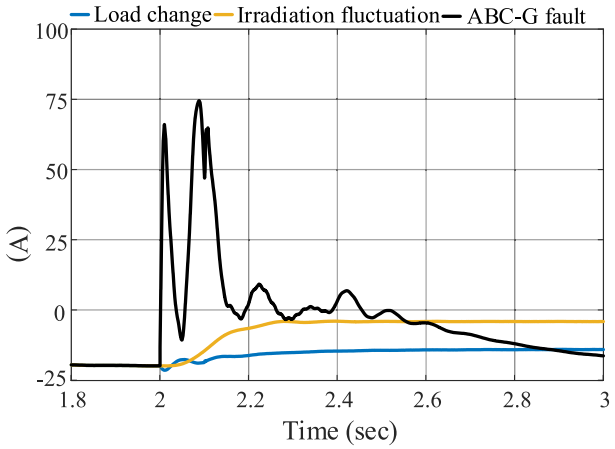

FIGURE 18. i_d curves measured with R5 for sudden load change, irradiation fluctuations, and ABC-G fault.

A. SUDDEN LOAD CHANGE

The proposed protection method is evaluated for a sudden change in load levels with a simultaneous 20% increase in the demand values for all loads in the microgrid at t=2s. Table.4 contains i_d values before and after load change and initial RoCoId in the first cycle after the load change. As an

example, the i_d curve and the variation of RoCoId for several relays in the upper and lower feeder of the test system are shown in Fig.13 and Fig.14 respectively. It can be observed that the measured values are significantly less than the preset threshold value with a margin of 83.54%, indicating an acceptable and safe room for secure distinguishing between erroneous and normal conditions.

B. IRRADIATION FLUCTUATIONS

Here, the robustness of the algorithm against fluctuations in irradiation is studied. The irradiation level for all PV systems in the microgrid is simultaneously reduced from $1000W/m^2$ to $500W/m^2$ at $t = 2s$. The diagram of i_d for R2, R5, and R8 in the upper feeder of the test system as well as R9, R12, and R15 in the lower feeder is shown in Fig.15. In addition, the variation of RoCoId for R5 and R12 during the occurrence of aforementioned scenario is shown in Fig.16. Furthermore, to evaluate the effectiveness of the proposed method in the presence of noise, a white Gaussian noise with the signal to noise ratio (SNR) of 20 dB was added to the measured signals in the microgrid. The variation of RoCoId for R11 with and without noise is shown in Fig.17, and the RoCoId values measured within a half cycle by all relays after the occurrence of the fluctuations in the presence of noise and without noise, are brought in Table.5. In these simulations, the maximum RoCoId measured with all relays is $118.4A/s$, which is 87.41% less than the preset threshold. This value is significantly less than the threshold value set for this microgrid. With this margin, irradiation fluctuations can properly be distinguished by the proposed protection from fault conditions. For the purpose of comparison, i_d curves measured with R5 are depicted in Fig.18 for some scenarios under investigation, i.e. sudden load change, irradiation fluctuations, and the occurrence of a three-phase to ground fault in the middle of L-3.

VI. CONCLUSION AND FUTURE RECOMMENDATION

This study proposes a new protection method based on the evaluation of the rate of change of i_d (RoCoId) to protect islanded inverter-based microgrids (IBMGs) containing both voltage-frequency controlled inverter-interfaced resources (VF-IIDER) and active-reactive power controlled inverter-interfaced resources (PQ-IIDER) as IBMG sources. This parameter contains high-frequency components in the transient state generated mainly by the converters and hence, can be deployed for protection purposes in non-quasi-static networks with low levels of inertia. The proposed method can be implemented in both centralized and decentralized approaches. The performance of the proposed protection method is validated by applying numerous cases, including symmetrical and asymmetrical faults with different resistances in various locations, as well as non-fault conditions such as sudden changes in demand levels and irradiation fluctuation scenarios, simulated on a test IBMG system in PSCAD/EMTDC environment. Moreover, the immunity of the proposed method under noisy measurement conditions has been proven. The obtained results indicate that the proposed protection method can efficiently distinguish between fault and non-fault conditions, and detect and discriminate the faulty part within a cycle of the supply frequency. In order to improve this work, further studies on high impedance fault (HIF) detection for islanded IBMGs, evaluation of communication reliability issues, and performance of the proposed method during multi-microgrids operation should be considered for future work.

REFERENCES

[1] X. Xu, F. Xue, S. Lu, H. Zhu, L. Jiang, and B. Han, "Structural and hierarchical partitioning of virtual microgrids in power distribution network," *IEEE Syst. J.*, vol. 13, no. 1, pp. 823–832, Mar. 2019.

[2] D. E. Olivares, A. Mehrizi-Sani, A. H. Etemadi, C. A. Canizares, R. Iravani, M. Kazerani, A. H. Hajimiragha, O. Gomis-Bellmunt, M. Saeedifard, R. Palma-Behnke, G. A. Jimenez-Estevez, and N. D. Hatziargyriou, "Trends in microgrid control," *IEEE Trans. Smart Grid*, vol. 5, no. 4, pp. 1905–1919, Jul. 2014.

[3] H. L. R. Van Der Walt, R. C. Bansal, and R. Naidoo, "PV based distributed generation power system protection: A review," *Renew. Energy Focus*, vol. 24, pp. 33–40, Mar. 2018.

[4] M. Norshahrani, H. Mokhlis, A. A. Bakar, J. Jamian, and S. Sukumar, "Progress on protection strategies to mitigate the impact of renewable distributed generation on distribution systems," *Energies*, vol. 10, no. 11, p. 1864, Nov. 2017.

[5] M. W. Altaf, M. T. Arif, S. N. Islam, and M. E. Haque, "Microgrid protection challenges and mitigation approaches—A comprehensive review," *IEEE Access*, vol. 10, pp. 38895–38922, 2022.

[6] L. Che, M. E. Khodayar, and M. Shahidehpour, "Adaptive protection system for microgrids: Protection practices of a functional microgrid system," *IEEE Electrific. Mag.*, vol. 2, no. 1, pp. 66–80, Mar. 2014.

[7] A. Hooshyar and R. Iravani, "Microgrid protection," *Proc. IEEE*, vol. 105, no. 7, pp. 1332–1353, Jul. 2017.

[8] H. Al-Nasseri, M. A. Redfern, and F. Li, "A voltage based protection for micro-grids containing power electronic converters," in *Proc. IEEE Power Eng. Soc. Gen. Meeting*, Jun. 2006, pp. 1–7.

[9] S. F. Zarei, H. Mokhtari, and F. Blaabjerg, "Fault detection and protection strategy for islanded inverter-based microgrids," *IEEE J. Emerg. Sel. Topics Power Electron.*, vol. 9, no. 1, pp. 472–484, Feb. 2021.

[10] W. Huang, T. Nengling, X. Zheng, C. Fan, X. Yang, and B. J. Kirby, "An impedance protection scheme for feeders of active distribution networks," *IEEE Trans. Power Del.*, vol. 29, no. 4, pp. 1591–1602, Aug. 2014.

[11] M. Dewadasa, A. Ghosh, G. Ledwich, and M. Wishart, "Fault isolation in distributed generation connected distribution networks," *IET Gener., Transmiss. Distrib.*, vol. 5, no. 10, p. 1053, 2011.

[12] B. Wang and L. Jing, "A protection method for inverter-based microgrid using current-only polarity comparison," *J. Modern Power Syst. Clean Energy*, vol. 8, no. 3, pp. 446–453, 2020.

[13] Z. Wang, L. Mu, and C. Fang, "Renewable microgrid protection strategy coordinating with current-based fault control," *J. Modern Power Syst. Clean Energy*, vol. 10, no. 6, pp. 1679–1689, 2022.

[14] C. Reiz and J. B. Leite, "Optimal coordination of protection devices in distribution networks with distributed energy resources and microgrids," *IEEE Access*, vol. 10, pp. 99584–99594, 2022.

[15] H. Beder, B. Mohandes, M. S. E. Moursi, E. A. Badran, and M. M. E. Saadawi, "A new communication-free dual setting protection coordination of microgrid," *IEEE Trans. Power Del.*, vol. 36, no. 4, pp. 2446–2458, Aug. 2021.

[16] M. Ojaghi and V. Mohammadi, "Use of clustering to reduce the number of different setting groups for adaptive coordination of overcurrent relays," *IEEE Trans. Power Del.*, vol. 33, no. 3, pp. 1204–1212, Jun. 2018.

[17] M. N. Alam, "Adaptive protection coordination scheme using numerical directional overcurrent relays," *IEEE Trans. Ind. Informat.*, vol. 15, no. 1, pp. 64–73, Jan. 2019.

[18] A. Arunan, T. Sirojan, J. Ravishankar, and E. Ambikairajah, "Real-time adaptive differential feature-based protection scheme for isolated microgrids using edge computing," *IEEE Syst. J.*, vol. 15, no. 1, pp. 1318–1328, Mar. 2021.

[19] H. Muda and P. Jena, "Superimposed adaptive sequence current based microgrid protection: A new technique," *IEEE Trans. Power Del.*, vol. 32, no. 2, pp. 757–767, Apr. 2017.
[20] Z. Chen, X. Pei, M. Yang, L. Peng, and P. Shi, "A novel protection scheme for inverter-interfaced microgrid (IIM) operated in islanded mode," *IEEE Trans. Power Electron.*, vol. 33, no. 9, pp. 7684–7697, Sep. 2018.
[21] E. Casagrande, W. L. Woon, H. H. Zeineldin, and D. Svetinovic, "A differential sequence component protection scheme for microgrids with inverter-based distributed generators," *IEEE Trans. Smart Grid*, vol. 5, no. 1, pp. 29–37, Jan. 2014.
[22] D. P. Mishra, S. R. Samantaray, and G. Joos, "A combined wavelet and data-mining based intelligent protection scheme for microgrid," *IEEE Trans. Smart Grid*, vol. 7, no. 5, pp. 2295–2304, Sep. 2016.
[23] A. Soleimanisardoo, H. K. Karegar, and H. H. Zeineldin, "Differential frequency protection scheme based on off-nominal frequency injections for inverter-based islanded microgrids," *IEEE Trans. Smart Grid*, vol. 10, no. 2, pp. 2107–2114, Mar. 2019.
[24] W. T. El-Sayed, M. A. Azzouz, H. H. Zeineldin, and E. F. El-Saadany, "A harmonic time-current-voltage directional relay for optimal protection coordination of inverter-based islanded microgrids," *IEEE Trans. Smart Grid*, vol. 12, no. 3, pp. 1904–1917, May 2021.
[25] W. T. El-Sayed, E. F. El-Saadany, and H. H. Zeineldin, "Interharmonic differential relay with a soft current limiter for the protection of inverter-based islanded microgrids," *IEEE Trans. Power Del.*, vol. 36, no. 3, pp. 1349–1359, Jun. 2021.
[26] B. Patnaik, M. Mishra, R. C. Bansal, and R. K. Jena, "MODWT-XGBoost based smart energy solution for fault detection and classification in a smart microgrid," *Appl. Energy*, vol. 285, Mar. 2021, Art. no. 116457.
[27] M. Z. Daud, A. Mohamed, and M. A. Hannan, "Optimization of PI compensator parameters for grid-tied photovoltaic with energy storage systems using simplex algorithm," *Int. Rev. Model. Simul.*, vol. 5, no. 2, pp. 751–760, 2012.
[28] J. K. Tailor and A. H. Osman, "Restoration of fuse-recloser coordination in distribution system with high DG penetration," in *Proc. IEEE Power Energy Soc. Gen. Meeting-Convers. Del. Electr. Energy 21st Century*, Jul. 2008, pp. 1–8.
[29] Y. Sun, X. Hou, J. Yang, H. Han, M. Su, and J. M. Guerrero, "New perspectives on droop control in AC microgrid," *IEEE Trans. Ind. Electron.*, vol. 64, no. 7, pp. 5741–5745, Jul. 2017.
[30] Y. Levron, J. Belikov, and D. Baimel, "A tutorial on dynamics and control of power systems with distributed and renewable energy sources based on the dq0 transformation," *Appl. Sci.*, vol. 8, no. 9, p. 1661, Sep. 2018.
[31] J. Belikov and Y. Levron, "Comparison of time-varying phasor and dq0 dynamic models for large transmission networks," *Int. J. Electr. Power Energy Syst.*, vol. 93, pp. 65–74, Dec. 2017.
[32] W. K. A. Najy, H. H. Zeineldin, and W. L. Woon, "Optimal protection coordination for microgrids with grid-connected and islanded capability," *IEEE Trans. Ind. Electron.*, vol. 60, no. 4, pp. 1668–1677, Apr. 2013.

ABDOLHAMID FARSHADI received the B.Sc. degree in electrical engineering from Shiraz University, Shiraz, Iran, in 2018, and the M.Sc. degree in electrical engineering from the Amirkabir University of Technology, Tehran, Iran, in 2021. His research interests include power system protection, renewable energy integration, smart grids, and power electronics application in power systems.

BEHZAD KEYVANI EYDI received the B.Sc. degree from the Iran University of Science and Technology (IUST), Iran, in 2006, the M.Sc. degree from the University of Tehran, Iran, in 2009, and the Ph.D. degree in electrical engineering from University College Dublin (UCD), Ireland, in 2022. He is currently a Senior Power Systems Engineer with Mott Macdonald Ltd., U.K. His research interests include power system analysis include transmission system planning and operation, protection, power system dynamics, and the integration of renewable generation into electrical networks.

HAMED NAFISI received the B.Sc., M.Sc., and Ph.D. degrees in electrical engineering from the Iranian Center of Excellence in Power Systems, Amirkabir University of Technology, Tehran, Iran, in 2006, 2008, and 2014, respectively. He is currently a Research Fellow with the School of Electrical and Electronic Engineering, Technological University Dublin (TU Dublin). His current research interests include smart grids, peer-to-peer energy trading, electric vehicles, power system protection, and power electronics application in power systems.

HOSSEIN ASKARIAN-ABYANEH (Member, IEEE) received the B.S. degree in electrical engineering from the Iran University of Science and Technology, in 1976, the M.S. degree from Tehran University, Tehran, Iran, in 1982, and the M.S. and Ph.D. degrees in power engineering from The University of Manchester Institute of Science and Technology, Manchester, U.K., in 1985 and 1988, respectively. Currently, he is a Professor with the Department of Electrical Engineering, Amirkabir University of Technology, Tehran. He has published numerous scientific papers in reviewed journals and presented at international conferences. His research interests include power system protection and power quality.

ARASH BEIRANVAND (Member, IEEE) received the B.Sc. degree in electrical engineering power systems from Guilan University, Rasht, Iran, the M.Sc. degree in electrical engineering power systems from the Shahid Beheshti University, Tehran, Iran, and the Ph.D. degree in electrical engineering from University College Dublin, in 2021. Currently, he is a Lecturer (Asst) with Technological University Dublin. Prior to that, he was a Research Fellow with the Energy Institute, University College Dublin. His research interests include the topological features of power grids, the optimization of electrical energy systems, the assessment of power grids resilience, and the operational vulnerabilities of power systems.